A μNMR CMOS Transceiver Using a Butterfly-Coil Input for Integration with a Digital Microfluidic Device Inside a Portable Magnet

Ka-Meng Lei, Pui-In Mak, Man-Kay Law and Rui P. Martins [1]

The State Key Laboratory of Analog and Mixed-Signal VLSI and FST-ECE, University of Macau, Macao, China
1 – On leave from Instituto Superior Técnico, Universidade de Lisboa, Portugal
E-mail Correspondence: pimak@umac.mo

***Abstract*—This paper reports a CMOS transceiver apt for integration with a digital microfluidic device, allowing electronic-automated sample management and measurement of micro-nuclear magnetic resonance (μNMR) signals inside a portable magnet. The transmitter (TX) employs an all-digital state control and a pulse sequence synthesizer to emit the exciting pulses for the samples. The receiver (RX) is led by a low-noise amplifier (LNA) using multi-stage NMOS-PMOS-complementary differential pairs, to achieve a sub-nV/√Hz input-referred noise. The RX baseband is a 6th-order Butterworth, dynamic-baseband-bandwidth lowpass filter (2.5 to 20 kHz), which suppresses the out-of-band noise and offers a fast recovery time between the exciting pulses, reducing the dead time of the RX for better sensitivity. Fabricated in 0.18-μm CMOS, the transceiver occupies a die area of 2.1 mm² and consumes 6.6/23.7 mW of power in the TX/RX mode.**

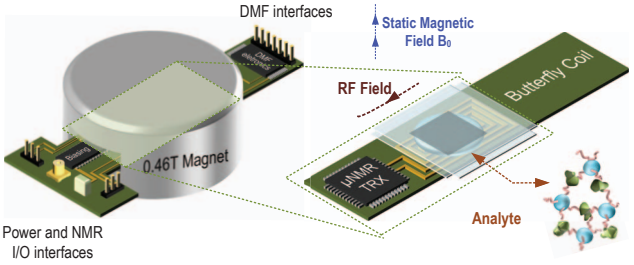

Fig. 1 A portable electronic-automated μNMR relaxometer. It features an inside-magnet μNMR CMOS transceiver (TRX) and a PCB-based Butterfly-Coil to transduce between magnetic and voltage signals. The analyte is placed inside a digital microfluidic (DMF) device on top of the Butterfly-coil for sample management.

I. Introduction

Rapid and accurate characterization of biological target, such as viruses, DNA, proteins and bacteria, can significantly improve the efficiency in combating human infections. The traditional detection techniques such as qPCR (qualitative polymerase chain reaction, for DNA) and ELISA (enzyme-linked immunosorbent assay, for antibodies/antigens) have to be performed in clinical laboratories, limiting their usages in outdoor. On the other hand, a portable and low-cost diagnostic platform that does not rely on benchtop laboratory equipment with minimal sample purification and processing can be employed for early screening of different diseases, rendering it as a promising solution in developing countries.

Initiated by the advances of CMOS, a wide variety of portable diagnostic tools built on semiconductor have been reported [1, 2]. Nuclear magnetic resonance (NMR), which principle is the exchange of energy between the RF magnetic field and precession of the non-zero spin nuclei (i.e., ^{1}H, ^{13}C, ^{31}P, etc.) at the presence of a static magnetic field applied on the nuclei, provides a non-invasive and rapid solution for Point-of-Care diagnosis. Firstly reported in 2002 [3], the NMR-based bio-sensing entailing magnetic nanoparticles probes has been developed to detect a wide range of unprocessed target such as DNA [3], pathogens [4], proteins [5] and cancer markers [6], by measuring the spin-spin relaxation time (T_2) of the protons. However, as the NMR-signal's amplitude is proportional to the square of the static magnetic field strength, a prodigious super-conducting magnet (B > 1 T) was required. Recently, several micro-NMR (μNMR) systems focusing on miniaturizing the size and weight of the magnet have been implemented in CMOS for applications in relaxometry (nuclei relaxation times) [6] and spectroscopy (NMR spectrum) [7]. The portability of the magnets (weight < 7.3 kg) and simplicity of the readout electronics render these μNMR systems suitable for Point-of-Care diagnosis.

This paper reports a CMOS transceiver suitable for μNMR relaxometry measurements inside a portable magnet (0.46 T, 1.25 kg), and can be integrated with a digital microfluidic (DMF) device for sample management (Fig. 1). The transceiver interfaces with a PCB-based Butterfly-coil to transduce between the magnetic and voltage signals inside the limited space of the magnet. To prevent human error and sample contamination, and to enable timing control of each reaction for multi-step protocols, the DMF device is integrated with the transceiver so that electronic-automated measurements can be achieved [8].

II. System Design

A. CMOS μNMR Transceiver with a Butterfly-Coil-Input

The schematic of the entire μNMR relaxometer is depicted in Fig. 2. The μNMR transceiver interfaces with a Butterfly-coil to transduce the AC magnetic field to/from the voltage signals. Unlike the typical spiral coil, such a Butterfly-coil can optimize the space inside the magnet by generating a plane-parallel RF magnetic field between the centers of the coil, which is orthogonal to the static magnetic field of the magnet. A capacitor C_{ext} is connected in parallel with the Butterfly-coil to form a LC resonator at proton's Larmor frequency (~20 MHz at 0.46 T) for passive amplification with a gain of $\sqrt{Q^2+1}$ [6]. This scheme is viable attributed to the narrow bandwidth of the NMR signals (<5 kHz). For the TX, an all-digital state control and pulse sequence synthesizer is utilized to generate the Carr-Purcell-Meiboom-Gill (CPMG) pulse sequences (Fig. 3) to precess the protons at their Larmor frequency, and refocus the incoherent magnetization across the samples caused by the inhomogeneous magnetic field inside the magnet. The power

978-1-4673-7191-9/15/$31.00 ©2015 IEEE

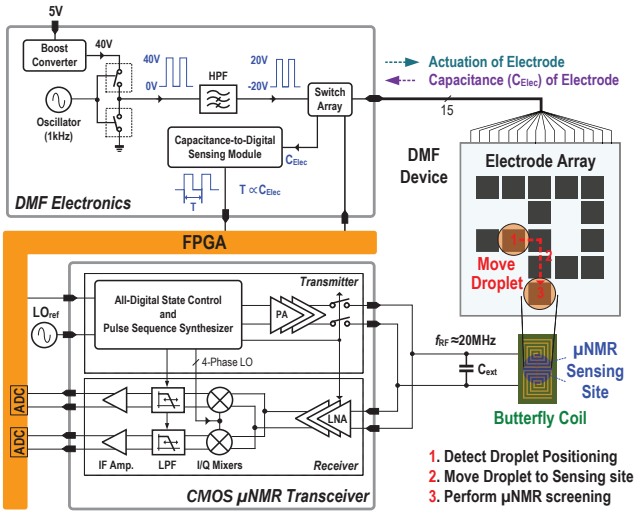

Fig. 2 Schematics of the μNMR relaxometer including the Butterfly-Coil-input CMOS μNMR transceiver, the DMF control electronics and their connections with the DMF device.

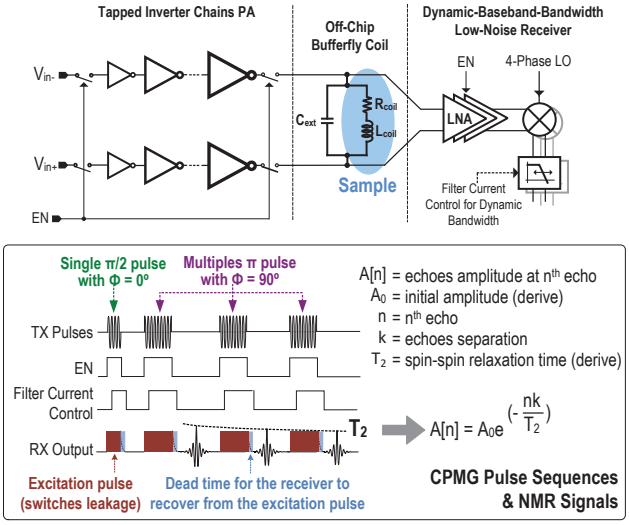

Fig. 3 Operating models of the dynamic baseband bandwidth inside the CMOS transceiver, and the corresponding NMR pulse sequence, including the CPMG pulse, NMR output signal and filter current control.

amplifier is made of tapped inverter chains (Fig. 3) to drive up the Butterfly-coil, featuring high dynamic power efficiency and low static power.

To maximize the RX sensitivity, it is headed by a multi-stage NMOS-PMOS complementary differential-pair LNA to amplify the induced voltage across the Butterfly-coil. This current-reuse topology allows a very low input-referred noise. To circumvent the substrate noise coupling from the digital circuits, the NMOS input pairs are segregated from the p-type substrate with a deep N-well. AC-coupling is inserted between the LNA stages to avoid the accommodated dc-offset from saturating the RX. Subsequent to the LNA, the I/Q mixers are based on the double-balanced Gilbert cell with RF transconductance sharing. They down-convert the NMR signals to baseband (bandwidth <5 kHz). The Gilbert cell features high conversion gain and port-to-port isolation, whereas the input RF transconductance sharing stage improves the I/Q balancing. The baseband LPF suppresses the high-frequency products of the mixing as well as the out-of-band noises. Theoretically, the bandwidth of the filter should be at the minimum (i.e., 5 kHz). Yet, the exciting pulses caused by the switches leakage will saturate the LPF, and create a dead-time for the RX after these excitation pulses. This dead-time, which is inversely proportional to the bandwidth of the LPF, limits the shortest interval between the echoes of the CPMG pulses and hence the number of achievable echoes within the echoes train. The sensitivity of the experiment is confounded by this dead-time, especially for the samples with short T_2 [9]. To circumvent this barrier, a dynamic-baseband-bandwidth LPF is proposed to alleviate the trade-off between fast recovery time from the excitation pulses in the TX mode, and minimum bandwidth in the RX mode by switching the bias current of the LPF. The LPF's bias current is dynamically tuned by the state control and slightly delayed from the exciting pulses (Fig. 3) for fully recovering after the exciting pulses. The LPF is based on cascaded source-follower-based Biquad cells, which bandwidth is directly tuned by the bias current (thus the transconductance). This topology is also power efficient as it can synthesize complex poles in a single branch by using transistorized positive feedback, avoiding any parasitic poles. A pair of IF amplifiers are placed subsequent to the LPF to drive the off-chip circuitry (ADC). The entire transceiver is shut down when idling to reduce the static power consumption.

B. DMF Device and Electronics

The DMF device is to enable sample management inside the small gap (32 mm x 14 mm) of the portable magnet. Unlike conventional microfluidic solutions, our DMF here can avoid separated laboratory gadgets (i.e., pumps and valves), rendering it as a promising solution for sample manipulation. By utilizing the principle of electrowetting-on-dielectric, the surface tension of the electrode can be modulated by applying voltage signals (~40 V, square wave) on the corresponding electrode where the droplet sample is to move in. Thus, sample movement inside the DMF device can be electronically accomplished, culminating an electronic-automated multi-sample management scheme to eliminate laboring efforts and the risks of defilement. A shell of silicone oil covers the droplet to smoothen the motion and prevent sample evaporation. The Indium Tin Oxide coated substrate and Chromium electrode of the DMF device are designed to have minimum impact on the Eddy Current loss of the Butterfly-coil attributed to the conductivity of the DMF device, preventing the NMR signals from exacerbation.

The DMF device is controlled by the DMF electronics module. A DC-DC converter produces the high voltage for driving the DMF device. A pair of switches driven by an oscillator (~1 kHz) is utilized to generate the square wave driving up the electrodes. A FPGA is employed to control the signal applied on each electrode for mastering the location of the droplet. Also, a capacitance-to-digital module is realized to sense the positions of the droplets as the droplets altered the capacitance of the electrodes (C_{Elec}). The entire DMF module forms a closed-loop control to govern the movement of the droplets and prevent unintentional mixing. The overall μNMR relaxometer, including the path of the droplet and the operation of the μNMR assays is mastered by the FPGA, which is linked with the PC for setting the parameters of the experiments and displaying real-time μNMR assay results. The DMF module is switched off during μNMR assay to prevent crosstalk on the μNMR results.

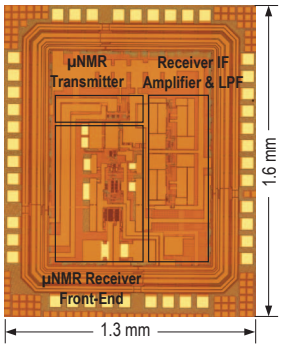

(a)

Process	CMOS 0.18 μm 6M1P
Voltage	1.8 V
Power Consumption	RX: 23.7 mW
	TX: 6.6 mW
TX efficiency	27.5 %
RX Input-Referred Noise*	0.92 nV/√Hz
RX Gain and Passband Bandwidth*	87.6 dB
	2 to 33 MHz
LPF	Bandwidth: 2.5 to 20 kHz
	Settling Time: 0.1 to 0.4 ms

*Extracted from simulation as the RX is interfaced with the Butterfly-Coil

(b)

Fig. 4 (a) Chip photo and (b) Performances of the μNMR transceiver. The RX input-referred noise, gain and bandwidth can only be assessed by simulations as the RX input has been tied to the butterfly-coil.

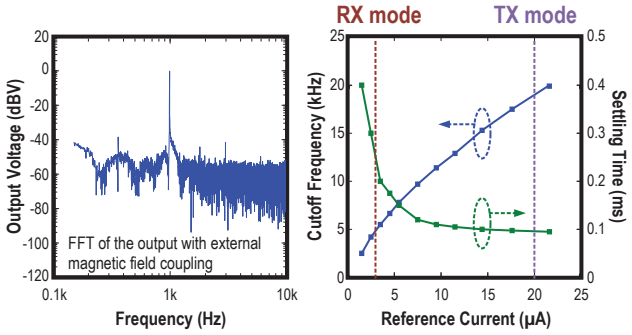

(a) (b)

Fig. 5 (a) RX output spectrum under an external magnetic field at 19.999 MHz and a LO of 20 MHz; (b). Cutoff frequency and settling time of the LPF versus the bias reference current. The working region of the LPF at different mode are labeled.

III. Simulation and Experimental Results

A. CMOS Transceiver with Butterfly-Coil-Input

The Butterfly-coil was fabricated on PCB with conductor width and spacing of 6 mil, respectively. The number of turns of the coil is optimized according to the input-referred noise of the receiver and the optimum turns is derived as 7 (per loop). The measured inductance of the Butterfly-Coil is 373 nH with a quality factor of 31.0 at 20 MHz.

The CMOS μNMR transceiver was fabricated in a 0.18-μm CMOS process with a die area of 1.6 x 1.3 mm^2. The chip photo is shown in Fig. 4(a). The measured power consumption of the TX is 6.6 mW, with an efficiency of 27.5% where most of the power is dissipated at the power amplifier. The effective RF magnetic field applied on the sample is 5.3 Gauss. The RX consumes 23.7 mW of power, which is dominated by the forefront LNA (68%). The transceiver is suitable for portable applications (e.g., with battery powering) albeit its relatively high power consumption in RX mode as the overall system is shut down (~100 μW) after the assay. Each assay takes only 1.1 s (for echoes interval of 4 ms and 256 echoes). With two AA batteries and a DC-DC converter of 90% efficiency, the system can complete ~1 million assays.

The simulated gain of the RX is 87.6 dB with an input-referred noise of 0.92 nV/√Hz at 20 MHz. The functionality of the RX is experimentally verified by applying a magnetic field near the Butterfly-Coil, imitating the magnetic field generated by the protons. With an external magnetic field of 19.999 MHz and a LO of 20 MHz, the RX responses a sinusoidal output at 1 kHz, as illustrated in Fig. 5(a). The experiments are repeated with the DMF device covering the Butterfly-Coil and no perceivable effect occurs on the output. This result verifies that the conductivity of the DMF device have negligible impact on the CMOS transceiver using a Butterfly-coil-input.

The response from the LPF is characterized by measuring the cutoff frequency and settling time of the LPF, as shown in Fig. 5(b). The achievable cutoff frequency of the LPF ranges from 2.5 to 20 kHz, which is commensurate with the reference current (from 1.5 to 21.5 μA). Correspondingly, the settling time of the LPF from an input step decreased from 0.4 to 0.1 ms. By dynamically altering the bias current (i.e., 3 μA in RX mode and 20μA in TX mode), short dead-time after the TX mode and low in-band noise in the TX mode are concurrently achieved. The overall relaxometer (without magnet) is shown in Fig. 6(a).

B. Proton μNMR Experiments

The μNMR assays are performed on protons of ^1H atoms in the water samples (8 μL) within the DMF device. Spacing between the echoes were set to 4 ms for all cases and the experiments were repeated 8 times to suppress the noise and distortion from the results. The sample is placed at an arbitrary position inside the DMF device and the location can be sensed by the capacitance-to-digital module. Afterwards the μNMR relaxometer transports the sample to the μNMR sensing site sequentially by applying actuating voltage on the Chromium electrodes with an average velocity of 1.17 mm/s, illustrated in Fig. 6(b) and (c). The speed can be enhanced at the expense of lower reliability of the device attributed to the higher chance of dielectric breakdown. As speed is not a major issue in the system, a lower driving voltage (40 V_{pp}) is adopted. Upon the samples arrived the μNMR sensing site, the μNMR assays will be triggered automatically. The resulting I/Q NMR signals are digitized by two ADCs and the computer analyzes and extracts the T_2 of the samples, as illustrated in Fig. 6(d) from pure water. The echoes from the NMR signal form an envelope decaying exponentially with a time constant T_2, which is the spin-spin relaxation time of the samples. The T_2 of the samples can be derived by fitting the resultant envelope with the exponential function. For instance, the T_2 of water is derived as 1.16 ± 0.03 s.

The μNMR relaxometer is able to quantify the target inside the water samples. With paramagnetic Copper (II) ions, the spin-spin relaxation rate ($1/T_2$) of the sample is commensurate with the concentration of Copper (II) ions (slope: 1.05 $s^{-1}mM^{-1}$; R^2: 0.998) thus the concentration of the Copper (II) ions can be pinpointed from the T_2 of the samples.

The system is also capable to detect biological target using target-specific probe-decorated magnetic nanoparticles. Existence of the targets inside the sample leads to formation of nanoparticle micro-clusters. Since the relaxation rate of water depends on the size and magnetization of the magnetic nanoparticles inside, the nanoparticle micro-clusters can be viewed as single nanoparticles with stronger magnetization, resulting in the deviation of T_2, which is proportional to the amount of target, upon the binding between the target and probe-decorated magnetic nanoparticles. To exemplify it, avidin and biotinylated nanoparticles ([Fe] = 0.5 mM, Ø = 30 nm) are used as analyte and probe, respectively. Attributed to the low dissociation constant of biotin and avidin (~10^{-15} M), the biotinylated nanoparticles form nanoparticle micro-clusters upon the addition of avidin. The probe and analyte are placed

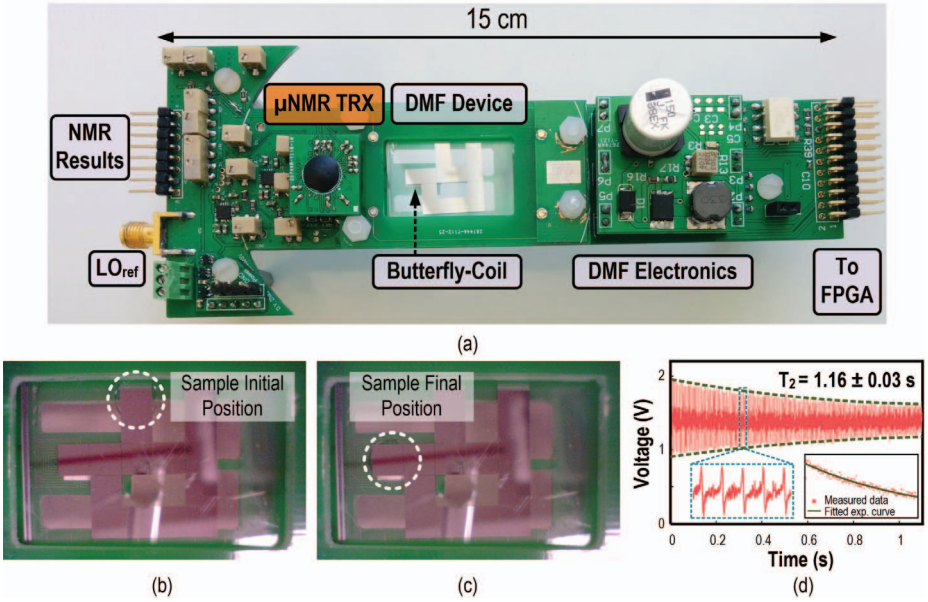

Fig. 6 (a) The system hardware of the μNMR relaxometer (without the magnet); (b) Initial position of the sample inside the DMF device. (c) Final position of the sample (on the μNMR sensing site), transported electronically from the initial position. (d) The acquired NMR signal from water excited by CPMG pulse with 256 echoes. The extracted envelope from the NMR signal is fitted by the mono-exponential function, as shown in the inset.

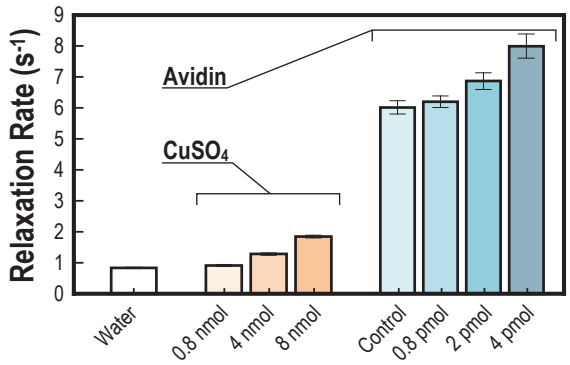

Fig. 7 Relaxation rate from samples contained Copper (II) ions and avidin with biotinylated nanoparticles.

inside the DMF device separately. The probe is guided and mixed with the analyte. Afterwards, the mixture is transported to the μNMR sensing site for assay. The T_2 of the samples is linearly correlated with the amount of avidin (slope: -42.5 $s \cdot mM^{-1}$; R^2 of 0.993) with a high detection sensitivity of 0.8 pmol. The relaxation rate from different concentrations of Copper (II) ions and avidin with biotinylated nanoparticles as probes are shown in Fig. 7.

IV. Conclusions

A CMOS transceiver using an all-digital TX and a dynamic-baseband-bandwidth RX for μNMR relaxometry measurements is reported. The TX excites the atoms via the Butterfly-coil and the RX amplifies the resultant NMR signals and down-convert them into the baseband for subsequent processing. The LPF features a dynamic bandwidth to achieve low in-band noise in RX mode and short dead-time in the TX mode. The samples under assay are managed electronically by the DMF device, reducing the change of sample defilement. Protons μNMR experiments were performed on Copper (II) ions and avidin-biotinylated magnetic nanoparticles, evincing that the system is beneficial to the development of rapid and portable diagnostic tools.

ACKNOWLEDGEMENT - This research is funded by the Macau Science and Technology Development Fund (FDCT) under the project (047/2014/A1) and State Key Lab fund.

References

[1] H. M. Jafari, K. Abdelhalim, L. Soleymani, E. H. Sargent, S. O. Kelley, and R. Genov, "Nanostructured CMOS Wireless Ultra-Wideband Label-Free PCR-Free DNA Analysis SoC," *IEEE J. Solid-State Circuits,* vol. 49, no. 5, pp. 1223-1241, May 2014.

[2] Y.-J. Huang *et al.*, "A Self-Powered CMOS Reconfigurable Multi-Sensor SoC for Biomedical Applications," *IEEE J. Solid-State Circuits,* vol. 49, no. 4, pp. 851-866, Apr. 2014.

[3] J. M. Perez, L. Josephson, T. O'Loughlin, D. Högemann, and R. Weissleder, "Magnetic relaxation switches capable of sensing molecular interactions," *Nature Biotechnology*, vol. 20, pp. 816–820, Aug. 2002.

[4] M. Liong *et al.,* "Magnetic barcode assay for genetic detection of pathogens," *Nature Communications*, vol. 4, pp.1-9, Apr. 2013.

[5] H. Lee, E. Sun, D. Ham, and R. Weissleder, "Chip-NMR biosensor for detection & molecular analysis of cells," *Nature Medicine*, vol. 14, no. 8, pp. 869–874, Aug. 2008.

[6] N. Sun, T.-J. Yoon, H. Lee, W. Andress, R. Weissleder, and D. Ham, "Palm NMR and 1-chip NMR," *IEEE J. Solid-State Circuits,* vol. 46, no. 1, pp. 342-351, Jan. 2011.

[7] D. Ha, J. Paulsen, N. Sun, Y.-Q. Song, and D. Ham, "Scalable NMR spectroscopy with semiconductor chips, " *Proc. Nat. Acad. Sci. (PNAS),* vol. 111, no. 33, pp. 11955-11960, Aug. 2014.

[8] K.-M. Lei, P.-I. Mak, M.-K. Law, and R. P. Martins, "A palm-size μNMR relaxometer using a digital microfluidic device and a semi-conductor transceiver for chemical/biological diagnosis," *Analyst*, vol. 140, pp. 5129-5137, Aug. 2015.

[9] J. Watzlaw, S. Glöggler, B. Blümich, W. Mokwa, and U. Schnakenberg, "Stacked planar micro coils for single-sided NMR applications," *J. of Magentic Resonance*, vol. 230, pp. 176-185, May 2013.